

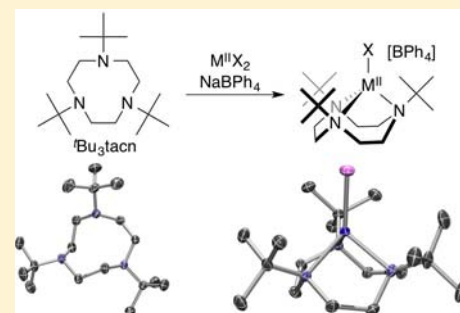
1,4,7-Triazacyclononane Ligands Bearing Tertiary Alkyl Nitrogen Substituents

Arumugam Thangavel, Marika Wieliczko, John Bacsá, and Christopher C. Scarborough*

Department of Chemistry, Emory University, Atlanta, Georgia 30322, United States

S Supporting Information

ABSTRACT: The first synthesis of 1,4,7-tri-*tert*-butyl-1,4,7-triazacyclononane (^tBu₃tacn) and its adamantyl analog Ad₃tacn are described. Cr^{II}, Mn^{II}, Fe^{II}, Co^{II}, Ni^{II}, and Cu^I compounds of ^tBu₃tacn are reported: the steric properties of this ligand enforce four-coordinate geometries except in the case of five-coordinate Cr^{II}, enabling design of pseudotetrahedral compounds bearing this tridentate redox-inert ancillary ligand.



INTRODUCTION

1,4,7-Triazacyclononane (H₃tacn) and its N-substituted derivatives (R₃tacn) are textbook ligands for transition metals.^{1,2} With N–M–N angles near 90°, these facially binding ligands are ideal “caps” for octahedral metal centers. As a saturated, redox-inert, hard σ-only donor ligand, H₃tacn can support highly oxidizing metal centers (e.g., Ni^{III} and Mo^{VI}).³ Although H₃tacn supports six-coordinate environments for ions from groups 4–10, the bulkiest R₃tacn species reported to date, ^tPr₃tacn,⁴ typically enforces five-coordinate geometries when bound to these same metals.⁵ Remarkably, R₃tacn derivatives with tertiary alkyl R groups, which are likely to favor a four-coordinate pseudotetrahedral geometry, have not been reported. Given the success of related bulky tridentate ligands in supporting reactive four-coordinate terminal metal–oxo, –imido, and –nitrido (M(E)) moieties,⁶ as well as the rich history of saturated amine macrocycles supporting high-valent M(E) species,⁷ ^tBu₃tacn is an attractive target for supporting reactive M(E) moieties that are unusually stable to intramolecular decomposition. The absence of ^tBu₃tacn in the R₃tacn series is an artifact of synthetic routes used to access these ligands.

R₃tacn derivatives are generally synthesized by alkylation of H₃tacn, either with alkyl halides or by reductive amination. The standard H₃tacn synthesis is shown in Scheme 1.¹ This route precludes N-alkylation prior to cyclization, underscoring the

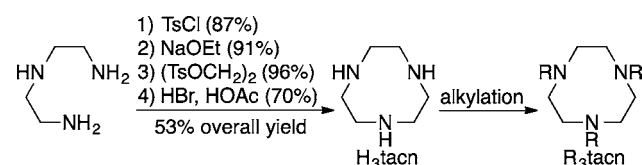
need for H₃tacn as a precursor to all R₃tacn derivatives. Effective methods for tertiary alkylation of secondary nitrogens are unavailable, precluding access to ^tBu₃tacn from H₃tacn. After more than 40 years of research on R₃tacn complexes,⁸ ^tBu₃tacn has remained inaccessible.

In this contribution, we describe the first synthesis of ^tBu₃tacn, which is carried out in three steps from commercially available reagents and employs crystallization as the sole means of purification. The related ligand, Ad₃tacn, is prepared by the same procedure. ^tBu₃tacn compounds of Mn^{II}, Fe^{II}, Co^{II}, and Ni^{II} are the first four-coordinate R₃tacn species of these metals. Five-coordinate [(^tBu₃tacn)(MeCN)Cr^{II}(OTf)][OTf] is likewise the lowest-coordinate R₃tacn chromium compound to date. [(^tBu₃tacn)Cu^I(MeCN)][PF₆] and [(Ad₃tacn)Cu^I(MeCN)][PF₆] are described and form the basis for a steric comparison of R₃tacn ligands.

EXPERIMENTAL SECTION

General Considerations. All reagents were purchased from either Sigma Aldrich or Strem Chemicals and were used as received unless noted otherwise. All metalation reactions were performed inside an MBRAUN UNILab 2000 inert-atmosphere glovebox. All anhydrous solvents (acetonitrile, methylene chloride, diethyl ether, pentane, and toluene) were purified and dried by an MBRAUN solvent purification system (SPS). ¹H and ¹³C NMR spectra were recorded at room temperature on Varian 300 or 400 MHz NMR spectrometers. IR spectra of neat compounds were recorded using a Nicolet 380 FT-IR (Thermo Electron Corporation). UV–vis/NIR absorption spectra were recorded on a Shimadzu UV-3600 spectrophotometer. Mass spectra were obtained from the Mass Spectrometry Center at Emory University. Elemental Analyses were obtained from Atlantic Microlab Inc., Norcross, Georgia. Solution-phase magnetic moments were

Scheme 1. Standard Route to H₃tacn and R₃tacn



Received: October 17, 2013

Published: November 4, 2013

measured by the Evans method.⁹ Cyclic voltammetry (CV) data were recorded on a Princeton Applied Research VersaSTAT 4 potentiostat.

Representative Ligand Synthesis: ^tBu₃tacn. *N,N'*-Bis(2-chloroacetyl)-*N,N'*-di-*tert*-butylethylenediamine (**2**). K₂CO₃ (44.11 g, 0.3191 mol) and methylene chloride (250 mL) were added to an oven-dried 250 mL round-bottom flask. *N,N'*-di-*tert*-butylethylenediamine (31.5 mL, 0.146 mol) was added at room temperature. After the flask was cooled in an ice bath, 2-chloroacetyl chloride (25.37 mL, 0.3191 mol) was added dropwise. As the addition progressed, the colorless solution became light yellow and turbid. The reaction was stirred over an ice bath for 3 h and then heated to 50 °C overnight. After the mixture cooled to room temperature, 50 mL of water was added and the organic layer was separated and washed with water (3 × 250 mL). After the solution was dried over MgSO₄ and filtered, the solvent was removed on a rotary evaporator. Crystallization of the crude residue from CH₂Cl₂/hexane afforded pure crystalline **2** in 68.9% yield (32.7 g). ¹H NMR (400 MHz, CDCl₃): δ 4.29 (s, 4H), 3.47 (s, 4H), 1.47 (s, 18H). ¹³C NMR (101 MHz, CDCl₃): δ 168.53, 57.24, 45.94, 43.73, 29.91. ESI-MS (*m/z*): calcd for {C₁₄H₂₆N₂O₂Cl₂ + H⁺}, 325.144 96; found, 325.144 56 (Δ = 1.2 ppm).

1,4,7-Tri-*tert*-butyl-1,4,7-triazocyclononane-2,6-dione (3**).** Sodium carbonate (50.0 g, 0.4765 mol) and **2** (62.00 g, 0.1906 mol) were combined in 2 L of anhydrous DMF in a 4 L one-neck round-bottom flask. The reaction mixture was heated at 120 °C for 1 h and then brought to room temperature. Neat *tert*-butylamine (22 mL, 0.2096 mol) was added, and the mixture was stirred at room temperature for 30 min and then heated at 120 °C for 3 days. The reaction mixture was brought to room temperature, and ~85% of the DMF solvent was removed on a rotary evaporator. Water (300 mL) was then added, and the mixture was stirred at room temperature for 1 h. Extraction with Et₂O and DCM, drying the combined organic extracts over MgSO₄, filtering, and removal of solvents under reduced pressure afforded the crude product, which was crystallized from ethyl acetate/hexane. This process afforded 41.7 g of pure crystalline **3** (67.3% yield). ¹H NMR (400 MHz, CDCl₃): δ 3.76 (s, 4H), 3.56 (s, 4H), 1.38 (s, 18H), 1.08 (s, 9H). ¹³C NMR (101 MHz, CDCl₃): δ 173.75, 63.96, 57.22, 56.39, 46.63, 28.59, 26.09. ESI-MS (*m/z*): calcd for {C₁₈H₃₅N₃O₂ + H⁺}, 326.280 75; found, 326.280 22 (Δ = 1.6 ppm).

^tBu₃tacn. Inside an inert-atmosphere glovebox, commercially available gray-colored LiAlH₄ (20.0 g) was suspended in 500 mL of dry Et₂O. The mixture was stirred overnight and filtered through a preweighed Celite pad. The gray-colored insoluble material (8.03 g) was discarded. (CAUTION! This material should be quenched very slowly by suspending it in an unreactive solvent (e.g., Et₂O) and slowly adding ^tPrOH to avoid ignition.) The colorless LiAlH₄ solution in diethyl ether (11.97 g) was used directly in the next step without isolation. **3** (33.0 g, 0.101 mol) was added portion-wise to the colorless homogeneous LiAlH₄ solution. As the addition progressed, the mixture became cloudy. The reaction was stirred at room temperature inside the glovebox overnight. The reaction mixture was then removed from the glovebox and successively quenched with 12, 24, and 36 mL of water, NaOH(aq) (10%), and water, respectively. The insoluble material was removed by filtration and discarded, the colorless solution was dried over MgSO₄ and filtered, and the solvent was removed on a rotary evaporator. The crude product was purified by crystallization from ethanol, affording 20.92 g of pure ^tBu₃tacn (69.7% yield) as colorless, X-ray quality crystals. ¹H NMR (300 MHz, CDCl₃): δ 2.62 (s, 12H), 0.98 (s, 27H). ¹³C NMR (101 MHz, CDCl₃): δ 54.68, 52.85, 26.98. ESI-MS (*m/z*): calcd for {C₁₈H₃₉N₃ + H⁺}, 298.3222; found, 298.3216 (Δ = 2.0 ppm).

Representative Procedure for the Synthesis of [(^tBu₃tacn)-M^{II}X][BPh₄]: M^{II}X = Mn^{II}Cl. ^tBu₃tacn (4.00 g, 0.1344 mmol), Mn^{II}Cl₂ (1.68 g, 0.1344 mmol), and sodium tetraphenylborate (13.8 g, 0.403 mmol) were combined in a 500 mL Schlenk flask with 300 mL of anhydrous acetonitrile. The heterogeneous suspension was stirred at room temperature, and over time the reaction mixture became pinkish-brown. The reaction was stirred overnight, after which time the solvent was removed in vacuo. The resulting viscous suspension was dissolved in anhydrous methylene chloride and stirred overnight. Filtration

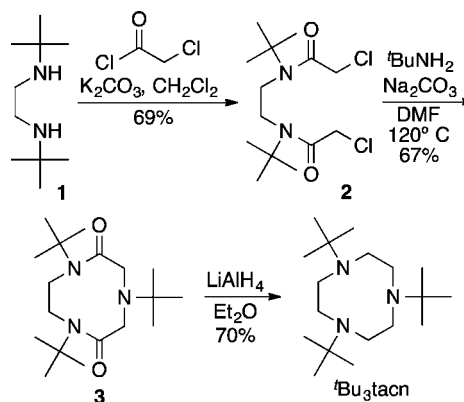
through a medium-porosity fritted funnel afforded a light-brown solution. The solvent was removed under vacuum, and the solid residue was washed with pentane and dried under vacuum. Analytically pure material was obtained by layering diethyl ether onto an acetonitrile solution of the product: 7.551 g (96.78%). X-ray quality crystals were grown from CH₂Cl₂/pentane. These crystals could be desolvated by heating under vacuum overnight. IR (neat, cm⁻¹): 543, 570, 611, 707, 732, 751, 812, 845, 877, 927, 998, 1031, 1047, 1080, 1135, 1187, 1229, 1286, 1374, 1404, 1418, 1476, 1577, 2162, 2979, 3053. Magnetic moment (Evans method, CD₃CN, 298 K): μ_{eff} = 5.6 μ_B. Anal. Calcd for C₄₂H₅₉BN₃ClMn: C, 71.34; H, 8.41; N, 5.94; Cl, 5.01. Found: C, 71.32; H, 8.35; N, 6.02; Cl, 4.88. ESI-MS (*m/z*): calcd for {C₁₈H₃₉N₃ClMn⁺}, 387.221 30; found, 387.220 27 (Δ = 2.6 ppm). ESI-MS (*m/z*): calcd for {C₂₄H₂₀B⁺}, 319.165 81; found, 319.168 89 (Δ = 9.6 ppm).

Representative Synthesis of [(R₃tacn)Cu^I(MeCN)][PF₆]: R = ^tBu. ^tBu₃tacn (1.0 g, 3.36 mmol) was suspended in 50 mL of anhydrous acetonitrile in a 100 mL Schlenk flask. [Cu(NCCH₃)₄][PF₆] (1.250 g, 3.36 mmol) was added, and the mixture was stirred at room temperature overnight. The reaction mixture was passed through a small pad of Celite, and the solvent was removed from the filtrate under vacuum. The residue was redissolved in methylene chloride and layered with pentane, providing 1.622 g of colorless X-ray quality crystals (88.6% yield). ¹H NMR (CD₃CN, 1.94 ppm): 2.975 (m, 6H), 2.49 (m, 6H), 2.30 (s, 3H), 1.26 (s, 27H). IR (neat, cm⁻¹): 551, 685, 729, 831, 877, 932, 1056, 1091, 1146, 1196, 1226, 1295, 1371, 1402, 1481, 2886, 2971. Anal. Calcd for C₂₀H₄₂N₄F₆PCu: C, 43.91; H, 7.74; N, 10.24; F, 20.84. Found: C, 43.89; H, 7.77; N, 10.13; F, 20.55. ESI-MS (*m/z*): calcd for {C₂₀H₄₂N₄Cu⁺}, 401.270 55; found, 401.270 48 (Δ = 0.2 ppm).

RESULTS AND DISCUSSION

We reasoned that synthesizing ^tBu₃tacn should proceed by preinstallation of *tert*-butyl groups on the nitrogens prior to cyclization because effective methods for alkylation of secondary nitrogens with tertiary alkyl groups are unavailable. Intrigued by reported methods for the synthesis of aza-crown compounds¹⁰ that were later applied to access the unsymmetrically substituted R₂R'^{tacn} derivatives Me₂R^{tacn} (R = norbornenylmethyl)¹¹ and Me₂B^{tacn},¹² we explored the synthesis of ^tBu₃tacn from commercially available *N,N'*-di-*tert*-butylethylenediamine (**1**), chloroacetyl chloride, and ^tBuNH₂ (Scheme 2). Diacylation of **1** with chloroacetyl chloride furnished intermediate **2** in 69% yield after crystallization from CH₂Cl₂/hexane. When combined with ^tBuNH₂ and Na₂CO₃ in DMF, **2** cyclized to diamide **3** in 67% isolated yield after crystallization from EtOAc/hexane. We encountered difficulties in the reduction of **3** due to low conversion or ring-opening. However, Et₂O-soluble LiAlH₄ cleanly reduced **3**

Scheme 2. Synthesis of ^tBu₃tacn



to ^tBu₃tacn, which was crystallized from EtOH in 70% yield (32% over three steps). The X-ray crystal structure of ^tBu₃tacn is shown in Figure 1. Although the yield of each step is modest,

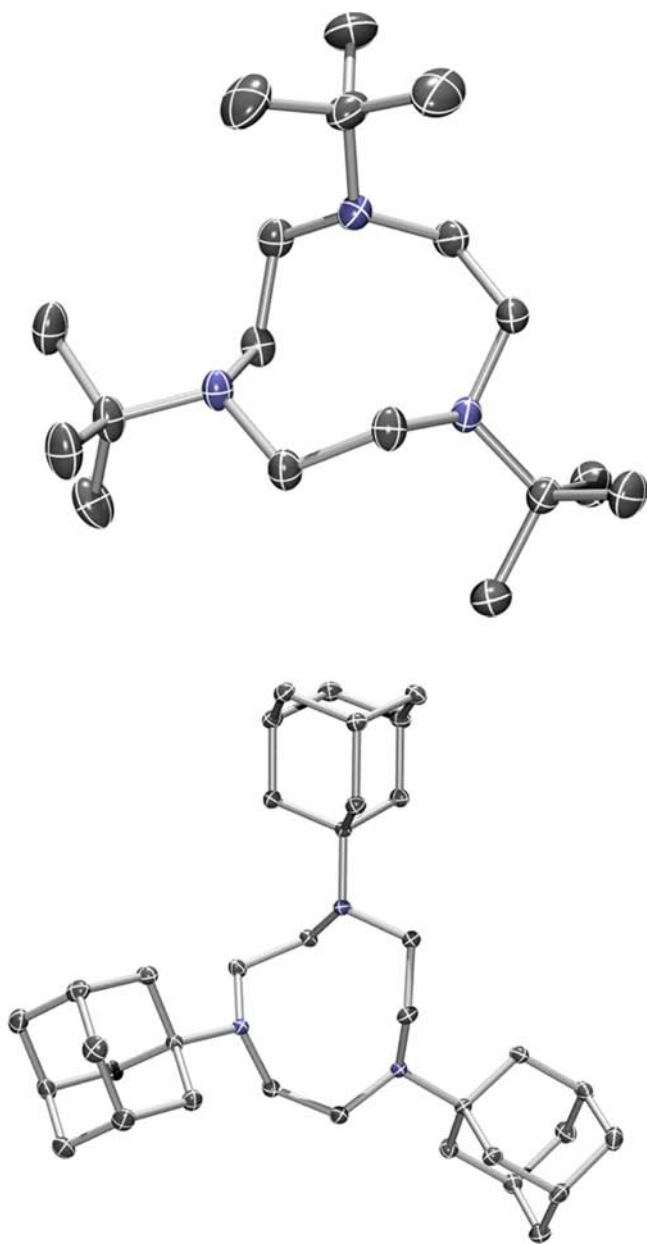


Figure 1. Solid-state molecular structures of ^tBu₃tacn (top) and Ad₃tacn (bottom). Hydrogen atoms are omitted for clarity.

the route has been scaled to afford 21g of ^tBu₃tacn in a single batch. By comparison, Me₃tacn is synthesized in five linear steps in 27% overall yield. Despite decades of synthetic inaccessibility, it appears that ^tBu₃tacn is among the most easily accessed N-substituted derivatives of H₃tacn owing to its three-step synthesis.

The route in Scheme 2 is amenable to the synthesis of Ad₃tacn, although each step is lower yielding (39%, 40%, and 57%, respectively); the crystal structure of this ligand is shown in Figure 1.¹³ Both ^tBu₃tacn and Ad₃tacn crystallize in an orientation where two nitrogen lone pairs project into the opposite face of the nine-membered ring than the lone pair of the third nitrogen, revealing that nitrogen inversion is a

prerequisite for coordination. The same orientation was observed in crystalline samples of Ts₃tacn¹⁴ and certain R₃tacn derivatives,¹⁵ and as with these ligands, the solid-state orientation does not inhibit the coordination of ^tBu₃tacn or Ad₃tacn to transition metals.

All known first-row transition-metal complexes of H₃tacn and R₃tacn in the Cambridge Structural Database,¹⁶ except those of copper and zinc, have crystallized in five-coordinate or higher geometries. A series revealing the steric influence of R in R₃tacn compounds on coordination number is depicted in Figure 2a.^{1,5a,b,d,17} Progressing in size of R results in a systematic

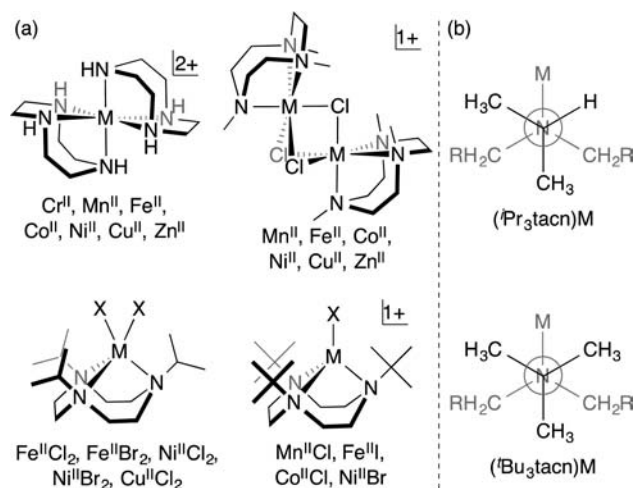


Figure 2. (a) Effect of R in R₃tacn on coordination environment of first-row transition metals as revealed by X-ray crystallography. (b) Newman projections along the R–N bond of the (R₃tacn)M unit demonstrating the solid-state orientation of the R groups in ^tPr₃tacn and ^tBu₃tacn.

change in observed coordination environment, with ^tPr₃tacn providing sufficient steric bulk to exclude a sixth ligand from the coordination sphere. In the solid-state geometry of five-coordinate ^tPr₃tacn complexes, the ^tPr groups project the H and one methyl of the tertiary carbon into the metal coordination sphere in a staggered conformation (Figure 2b). Replacement of ^tPr with ^tBu should result in substantial crowding by projecting two methyls per ^tBu group into the coordination sphere. Indeed, ^tBu₃tacn complexes of Mn^{II}, Fe^{II}, Co^{II}, and Ni^{II} are isolated as the first four-coordinate compounds of these metals bearing R₃tacn ligands, underscoring the pronounced size difference of ^tPr and ^tBu groups in these ligands.

The cations [(^tBu₃tacn)M^{II}X]⁺ were isolated as [BPh₄]⁻ salts by combining ^tBu₃tacn, MX₂, and NaBPh₄ in acetonitrile (Figure 3a). The solid-state molecular structure of the cation in [(^tBu₃tacn)Co^{II}Cl][BPh₄] is shown in Figure 3b; the structures of the remaining [(^tBu₃tacn)M^{II}X]⁺ salts are included in the Supporting Information. The average X–M–N and N–M–N angles for each species are shown in Figure 3c and reveal that the ligand is geometrically suited for facially capping an octahedron but sterically enforces a coordination number of four.

When ^tBu₃tacn and [Cr^{II}(OTf)₂·(MeCN)₂]¹⁸ are combined in CH₂Cl₂, the pseudomonovacant octahedral species [(^tBu₃tacn)(MeCN)Cr^{II}(OTf)][OTf] is isolated as blue-green crystals (Figure 4). This five-coordinate species is the lowest-coordinate crystallographically characterized R₃tacn chromium complex to date, highlighting again the unique steric environ-

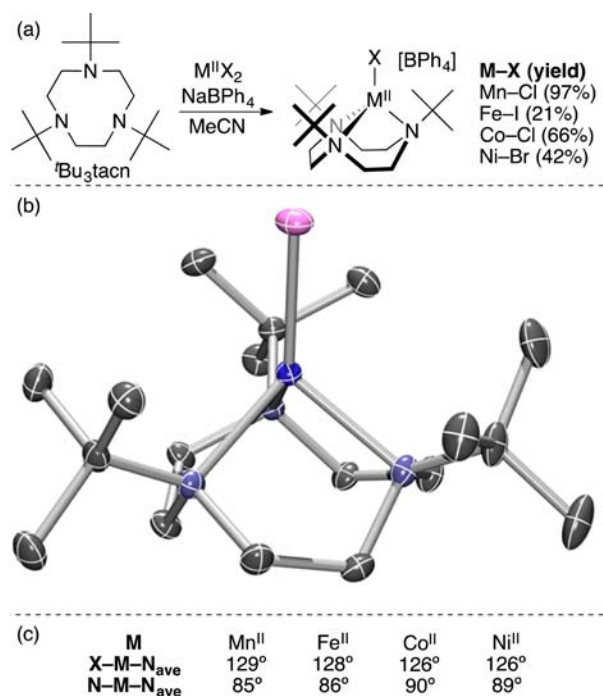


Figure 3. (a) Synthetic route to $[(t\text{Bu}_3\text{tacn})\text{M}^{\text{II}}\text{X}][\text{BPh}_4]$ compounds, with yields of isolated crystalline material given in parentheses. (b) Solid-state molecular structure of $[(t\text{Bu}_3\text{tacn})\text{Co}^{\text{II}}\text{X}][\text{BPh}_4]$. The counterion and H atoms are omitted for clarity. (c) Average X–M–N and N–M–N angles of each compound.

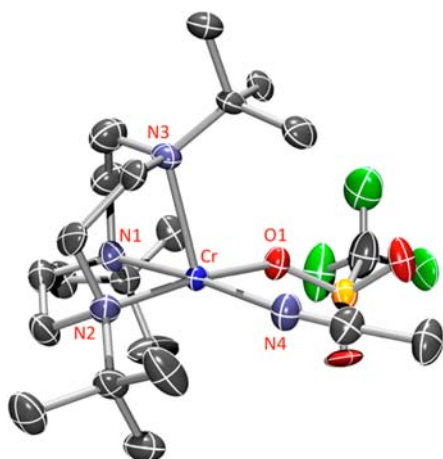


Figure 4. Solid-state molecular structure of the cation in $[(t\text{Bu}_3\text{tacn})(\text{MeCN})\text{Cr}^{\text{II}}(\text{OTf})][\text{OTf}]$. Counterion and H atoms are omitted for clarity. Selected bond lengths revealing axial elongation: Cr–N1 2.199(5) Å, Cr–N2 2.182(5) Å, Cr–N3 2.360(5) Å, Cr–N4 2.092(5) Å, and Cr–O1 2.062(4) Å.

ment imposed by $t\text{Bu}_3\text{tacn}$ among the R_3tacn ligands. The ability of this species to adopt a five-coordinate geometry stems from the electronic structure of high-spin Cr^{II} , which in a four-coordinate C_{3v} geometry is unstable to a first-order Jahn–Teller distortion by elongation of one Cr–N bond. Such an elongation opens the coordination sphere of the Cr^{II} ion enough to enable coordination of an acetonitrile ligand. The axial Cr–N_{tacn} bond (2.36 Å) is much longer than the equatorial Cr–N_{tacn} bonds (2.18 Å and 2.20 Å, Figure 4) as expected for a high-spin Cr^{II} species in this geometry. The Bu

groups on the equatorial $t\text{Bu}_3\text{tacn}$ nitrogens project into the empty axial coordination site, blocking access to a sixth ligand.

To quantify the steric environment imposed by R_3tacn ligands, we sought a transition metal that favors a four-coordinate geometry regardless of the identity of R. The four-coordinate cations $[(\text{R}_3\text{tacn})(\text{MeCN})\text{Cu}^{\text{I}}]^+$ (R = Me¹⁹ and $t\text{Pr}^{20}$) have been crystallographically characterized. $[(t\text{Bu}_3\text{tacn})(\text{MeCN})\text{Cu}^{\text{I}}][\text{PF}_6]$ and $[(\text{Ad}_3\text{tacn})(\text{MeCN})\text{Cu}^{\text{I}}][\text{PF}_6]$ were obtained by combining each ligand with $[(\text{MeCN})_4\text{Cu}^{\text{I}}][\text{PF}_6]$ in MeCN as crystalline material in 89% and 78% yield. The X-ray crystal structures of the cations in these species are shown

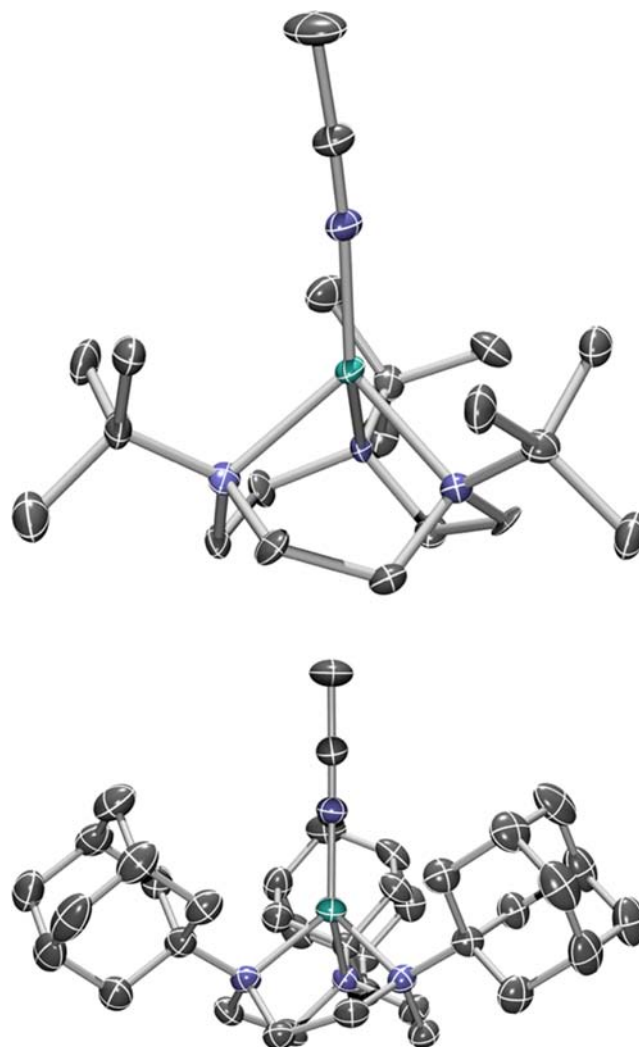


Figure 5. Solid-state molecular structures of the cations in $[(t\text{Bu}_3\text{tacn})(\text{MeCN})\text{Cu}^{\text{I}}][\text{PF}_6]$ (top) and $[(\text{Ad}_3\text{tacn})(\text{MeCN})\text{Cu}^{\text{I}}][\text{PF}_6]$ (bottom). H atoms and $[\text{PF}_6]^-$ counterions are omitted for clarity.

in Figure 5. The steric environments imposed by Me_3tacn , $t\text{Pr}_3\text{tacn}$, $t\text{Bu}_3\text{tacn}$, and Ad_3tacn in the solid-state structures of $[(\text{R}_3\text{tacn})(\text{MeCN})\text{Cu}^{\text{I}}]^+$ were quantified using the percent buried volume ($\%V_B$)²¹ method employed extensively as a steric probe of *N*-heterocyclic carbene ligands.²² This method calculates the percentage of the volume of a metal-centered sphere of defined radius that is occupied by a ligand. To focus the analysis on the nitrogen substituents, we have only included the nitrogen atoms and their substituents in the $\%V_B$

calculations. %V_B is shown in Figure 6 as a function of the radius of the copper-centered sphere. The %V_B is dominated by

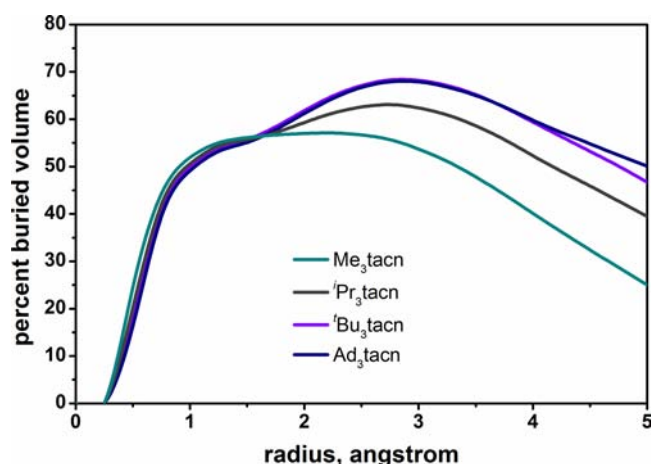


Figure 6. %V_B as a function of radius of a Cu^I-centered sphere in X-ray crystal structures of [(R₃tacn)(MeCN)Cu^I]⁺ species. Acetonitrile ligand, copper, counterion, and R₃tacn ethylene bridges are omitted in the calculated values.

the bound nitrogen atoms up to 1.5 Å, below which all ligands appear nearly isosteric. At larger radii, the nitrogen substituents begin to dominate the %V_B and reveal a notable increase in size from Me to ^tPr to ^tBu/^{Ad} in these ligands. [(^tPr₃tacn)(MeCN)Cu^I]⁺ crystallizes in an orientation in which one ^tPr group has both methyl groups gauche to the Cu–N bond (cf. Figure 2b), whereas the other two ^tPr groups have one methyl anti to the N–M bond.²⁰ This seems to be an artifact of the alleviated steric interactions associated with four-coordinate compounds of this type, as all five-coordinate ^tPr₃tacnM compounds have all three ^tPr groups in the orientation shown in the top of Figure 2b.⁵ In the solid state, ^tBu₃tacn and Ad₃tacn are clearly the bulkiest R₃tacn species to date based on both %V_B and the four-coordinate geometry enforced by ^tBu₃tacn (Figure 3). ^tBu₃tacn and Ad₃tacn are essentially isosteric within 4 Å of the copper center.

Sterically enforcing four-coordinate geometries can have a pronounced effect on compound redox properties and, by extension, stability of the accessible oxidation states. The relative redox potentials of [(H₃tacn)₂M^{II}]²⁺ and [(^tBu₃tacn)M^{II}X]⁺ for cobalt and nickel provide information about the effect of coordination number on metal redox activity. To avoid complicating redox noninnocence of [Ph₄B][−], we prepared [(^tBu₃tacn)M^{II}X][PF₆] (M^{II}X = Co^{II}Cl and Ni^{II}Br). These four-coordinate complexes are oxidized in electrochemically irreversible events at +1.03 and +1.07 V vs Fc/Fc⁺, respectively (Figure S3, Supporting Information), revealing that they are significantly more difficult to oxidize than the respective six-coordinate [(H₃tacn)₂M^{II}]²⁺ species (*E*_{1/2} = −0.81 and +0.55 V).^{3a,23} These ^tBu₃tacn species are also robust with respect to reduction: electrochemical reduction occurs at −1.81 and −1.60 V (Figure 7), demonstrating a wide potential window where the divalent oxidation state is favored. This contrasts a structurally related triphosphine Co^{II}I complex,²⁴ with reversible Co^I/Co^{II} and Co^{II}/Co^{III} couples at *E*_{1/2} = −0.92 and +0.01 V vs Fc/Fc⁺. We are currently exploring whether the redox stability endowed by ^tBu₃tacn on divalent transition-metal ions will enable isolation of M(E) species in unusually low oxidation states.²⁵

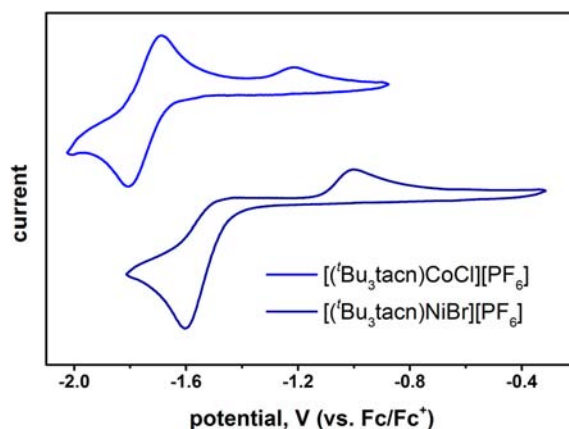


Figure 7. Cyclic voltammograms showing reductive events associated with [(^tBu₃tacn)Co^{II}Cl][PF₆] (top) and [(^tBu₃tacn)Ni^{II}Br][PF₆] (bottom). Conditions: 0.1 M [N(*n*Bu)₄][PF₆] in CH₃CN at 22 °C, 100 mV/s scan rate. Potentials are referenced to an internal ferrocene standard. Full potential sweeps are shown in Figure S3 (Supporting Information).

A description of the d-orbital splitting in [(^tBu₃tacn)M^{II}X]⁺ cations for metals from groups 6–11, derived from the angular overlap model, molecular orbital theory, and DFT calculations is provided in the Supporting Information. The conclusions from this analysis are summarized as follows:

- (1) The N–M–X angles (Figure 3c) are near the “magic angle” where the nitrogen lone pairs have no net overlap with the metal d_{z²} orbital, suggesting that the M–X bond is a pure two-center bond.
- (2) The d-orbital splitting is a 2-1-2 pattern for local C_{3v} symmetry, with the degenerate d_{xz}/d_{yz} orbitals most destabilized followed by d_{z²}.
- (3) These compounds are unstable to a large first-order Jahn–Teller distortion for Cr^{II} and Cu^{II}, and in each case the distorted geometry is intermediate between C_{3v} and a cis-divacant octahedron.

As discussed above, the structure of [(^tBu₃tacn)(MeCN)Cr^{II}(OTf)]⁺ can be viewed as derived from this Jahn–Teller distortion. The Fe^{II} species in local C_{3v} symmetry is also unstable to a Jahn–Teller distortion, but the unequally occupied degenerate orbitals in this case are approximately nonbonding, resulting in a very mild calculated distortion that is in good agreement with the crystal structure of [(^tBu₃tacn)Fe^{II}I][BPh₄] in which this species adopts a nearly ideal local C_{3v} geometry. High-spin d⁴ and d⁹ metal ions in local C_{3v} symmetry are unstable to a large Jahn–Teller distortion analogous to the same electron counts in octahedral symmetry characterized by a pronounced “static” Jahn–Teller distortion; high-spin d⁶[(^tBu₃tacn)Fe^{II}I]⁺ is analogous to high-spin d⁶ in octahedral symmetry that is characterized by a weak “dynamic” Jahn–Teller distortion. The DFT calculations are in good agreement with our crystallographic results and qualitative orbital descriptions, and these calculations provide the theoretical foundation that will guide our ongoing exploration of the coordination properties of ^tBu₃tacn.

CONCLUSIONS

We have described the first synthesis of ^tBu₃tacn and its Cr^{II}, Mn^{II}, Fe^{II}, Co^{II}, Ni^{II}, and Cu^I coordination compounds. Except for Cu, all species crystallize in the lowest-coordinate

environments to date for $R_3t\text{acn}$ compounds of these metals due to the steric influence of this bulky ligand. Both ${}^t\text{Bu}_3\text{tacn}$ and Ad_3tacn are significantly bulkier than the previously bulkiest $R_3\text{tacn}$ derivative, ${}^i\text{Pr}_3\text{tacn}$, and are essentially isosteric within a 4 Å coordination sphere. The low coordination number and hard nature of the nitrogen donors has a pronounced effect on the electrochemical properties of cobalt and nickel compounds of ${}^t\text{Bu}_3\text{tacn}$, as revealed by a much larger potential window wherein the divalent oxidation state is preferred compared to related compounds bearing a triphosphine ligand or two H_3tacn ligands. Our efforts have now turned to applying these redox-inert ${}^t\text{Bu}_3\text{tacn}$ and Ad_3tacn ligands to studies of reactive $M(E)$ units.

■ ASSOCIATED CONTENT

📄 Supporting Information

Remaining synthetic procedures and characterization data, details of crystallographic data collection and refinement, crystallographic information files in CIF format, remaining cyclic voltammograms, details of percent buried volume calculations, details of DFT calculations, theoretical treatment of $[({}^t\text{Bu}_3\text{tacn})M^{II}\text{Cl}]^+$ cations, and raw characterization data of organic and transition-metal compounds. This material is available free of charge via the Internet at <http://pubs.acs.org>.

■ AUTHOR INFORMATION

Corresponding Author

*C. C. Scarborough. E-mail: scarborough@emory.edu.

Notes

The authors declare no competing financial interest.

■ ACKNOWLEDGMENTS

C.S. gratefully acknowledges Emory University for providing the startup funds that supported this work. Dr. Fred Strobel is thanked for assistance with mass spectrometry.

■ REFERENCES

- (1) Chaudhuri, P.; Wieghardt, K. *Prog. Inorg. Chem.* **1987**, *35*, 329.
- (2) Wainwright, K. P. *Coord. Chem. Rev.* **1997**, *166*, 35.
- (3) (a) Wieghardt, K.; Schmidt, W.; Herrmann, W.; Kueppers, H. J. *Inorg. Chem.* **1983**, *22*, 2953. (b) McAuley, A.; Norman, P. R.; Olubuyide, O. *Inorg. Chem.* **1984**, *23*, 1938. (c) Wieghardt, K.; Walz, W.; Nuber, B.; Weiss, J.; Ozarowski, A.; Stratemeier, H.; Reinen, D. *Inorg. Chem.* **1986**, *25*, 1650. (d) Wieghardt, K.; Hahn, M.; Swiridoff, W.; Weiss, J. *Inorg. Chem.* **1984**, *23*, 94. (e) McGowan, P. C.; Podesta, T. J.; Thornton-Pett, M. *Inorg. Chem.* **2001**, *40*, 1445.
- (4) Haselhorst, G.; Stoetzel, S.; Strassburger, A.; Walz, W.; Wieghardt, K.; Nuber, B. *J. Chem. Soc., Dalton Trans.* **1993**, 83.
- (5) (a) Kawamura, M.; Sunada, Y.; Kai, H.; Koike, N.; Hamada, A.; Hayakawa, H.; Jin, R.-H.; Nagashima, H. *Adv. Synth. Catal.* **2009**, *351*, 2086. (b) Reilly, J.-N.; Charron, G.; Rivière, E.; Guillot, R.; Barra, A.-L.; Serrano, M. D.; van Slageren, J.; Mallah, T. *Chem.—Eur. J.* **2008**, *14*, 1169. (c) Han, W.; Li, L.; Liu, Z.-Q.; Yan, S.-P.; Liao, D.-Z.; Jiang, Z.-H.; Shen, P.-W. *Z. Anorg. Allg. Chem.* **2004**, *630*, 591. (d) Higashimura, H.; Kubota, M.; Shiga, A.; Fujisawa, K.; Moro-oka, Y.; Uyama, H.; Kobayashi, S. *Macromolecules* **2000**, *33*, 1986. (e) Halfen, J. A.; Tolman, W. B. *J. Am. Chem. Soc.* **1994**, *116*, 5475. (f) Halfen, J. A.; Hallman, J. K.; Schultz, J. A.; Emerson, J. P. *Organometallics* **1999**, *18*, 5435. (g) Diebold, A.; Elbouadili, A.; Hagen, K. S. *Inorg. Chem.* **2000**, *39*, 3915. (h) Halfen, J. A.; Mahapatra, S.; Wilkinson, E. C.; Gengenbach, A. J.; Young, V. G., Jr.; Que, L., Jr.; Tolman, W. B. *J. Am. Chem. Soc.* **1996**, *118*, 763.
- (6) Saouma, C. T.; Peters, J. C. *Coord. Chem. Rev.* **2011**, *255*, 920.
- (7) (a) McDonald, A. R.; Que, L., Jr. *Coord. Chem. Rev.* **2013**, *257*, 414. (b) Suh, Y.; Seo, M. S.; Kim, K. M.; Kim, Y. S.; Jang, H. G.;

Tosha, T.; Kitagawa, T.; Kim, J.; Nam, W. *J. Inorg. Biochem.* **2006**, *100*, 627. (c) Nam, W. *Acc. Chem. Res.* **2007**, *40*, 522. (d) Que, L., Jr. *Acc. Chem. Res.* **2007**, *40*, 493.

- (8) Koyama, H.; Yoshino, T. *Bull. Chem. Soc. Jpn.* **1972**, *45*, 481.
- (9) Evans, D. F.; Jakubovic, D. A. *J. Chem. Soc., Dalton Trans.* **1988**, 2927.
- (10) (a) Bradshaw, J. S.; Krakowiak, K. E.; Izatt, R. M. *Tetrahedron Lett.* **1989**, *30*, 803. (b) Bradshaw, J. S.; Krakowiak, K. E.; Izatt, R. M. *J. Heterocycl. Chem.* **1989**, *26*, 1431. (c) Krakowiak, K. E.; Bradshaw, J. S.; Izatt, R. M. *J. Org. Chem.* **1990**, *55*, 3364.
- (11) Grenz, A.; Ceccarelli, S.; Bolm, C. *Chem. Commun.* **2001**, 1726.
- (12) Belousoff, M. J.; Duriska, M. B.; Graham, B.; Batten, S. R.; Moubaraki, B.; Murray, K. S.; Spiccia, L. *Inorg. Chem.* **2006**, *45*, 3746.
- (13) CCDC 944691–944701 contain the supplementary crystallographic data for this paper. These data can be obtained free of charge from the Cambridge Crystallographic Data Centre via www.ccdc.cam.ac.uk/data_request.cif.
- (14) (a) Gott, A. L.; McGowan, P. C. *Acta Crystallogr.* **2003**, *E59*, o1702. (b) André, V.; Barroso, S.; Martins, A. M.; Duarte, M. T. *Acta Crystallogr.* **2007**, *C63*, o594.
- (15) (a) Adam, B.; Bill, E.; Bothe, E.; Goerdts, B.; Haselhorst, G.; Hildenbrand, K.; Sokolowski, A.; Steenken, S.; Weyhermüller, T.; Wieghardt, K. *Chem.—Eur. J.* **1997**, *3*, 308. (b) Moore, D. A.; Fanwick, P. E.; Welch, M. J. *Inorg. Chem.* **1989**, *28*, 1504. (c) Tei, L.; Blake, A. J.; Lippolis, V.; Wilson, C.; Schröder, M. *Dalton Trans.* **2003**, 304.
- (16) Allen, F. H. *Acta Crystallogr.* **2002**, *B58*, 380.
- (17) (a) Scarborough, C. C.; Sproules, S.; Weyhermüller, T.; DeBeer, S.; Wieghardt, K. *Inorg. Chem.* **2011**, *50*, 12446. (b) Bossek, U.; Nühlen, D.; Bill, E.; Glaser, T.; Krebs, C.; Weyhermüller, T.; Wieghardt, K.; Lengen, M.; Trautwein, A. X. *Inorg. Chem.* **1997**, *36*, 2834. (c) Steed, J. W.; Goeta, A. E.; Lipkowsky, J.; Swierczynski, D.; Panteleon, V.; Handa, S. *Chem. Commun.* **2007**, 813.
- (18) Hagen, K. S. *Inorg. Chem.* **2000**, *39*, 5867.
- (19) Bar-Nahum, I.; Gupta, A. K.; Huber, S. M.; Ertem, M. Z.; Cramer, C. J.; Tolman, W. B. *J. Am. Chem. Soc.* **2009**, *131*, 2812.
- (20) Berreau, L. M.; Halfen, J. A.; Young, V. G., Jr.; Tolman, W. B. *Inorg. Chem.* **1998**, *37*, 1091.
- (21) Poater, A.; Cosenza, B.; Correa, A.; Giudice, S.; Ragone, F.; Scarano, V.; Cavallo, L. *Eur. J. Inorg. Chem.* **2009**, *2009*, 1759.
- (22) Clavier, H.; Nolan, S. P. *Chem. Commun.* **2010**, 841.
- (23) Connelly, N. G.; Geiger, W. E. *Chem. Rev.* **1996**, *96*, 877.
- (24) Jenkins, D. M.; Peters, J. C. *J. Am. Chem. Soc.* **2005**, *127*, 7148.
- (25) MacBeth, C. E.; Thomas, J. C.; Betley, T. A.; Peters, J. C. *Inorg. Chem.* **2004**, *43*, 4645.